



# Tunable diode laser absorption spectroscopy for stable isotope studies of ecosystem–atmosphere CO<sub>2</sub> exchange

David R. Bowling<sup>a,\*</sup>, Steve D. Sargent<sup>b</sup>, Bert D. Tanner<sup>b</sup>, James R. Ehleringer<sup>a</sup>

<sup>a</sup> Stable Isotope Ratio Facility for Environmental Research, Department of Biology, University of Utah,  
257 South 1400 East, Salt Lake City, UT 84112-0820, USA

<sup>b</sup> Campbell Scientific Inc., 815 West 1800 North, Logan, UT 84321-1784, USA

Received 3 October 2002; received in revised form 20 March 2003; accepted 20 March 2003

## Abstract

The stable isotope content of atmospheric CO<sub>2</sub> provides information about ecosystem carbon–water relations and biosphere–atmosphere carbon exchange. Virtually every isotope study within these fields has required air sample collection at remote locations followed by isotope analysis at a laboratory. This requirement severely limits sampling frequency and experiment duration. In this paper, we evaluate a tunable diode laser absorption spectrometer (TDL) for measuring the carbon isotope content of CO<sub>2</sub> at atmospheric mole fractions (350–700 μmol mol<sup>-1</sup>) and isotopic abundance (δ<sup>13</sup>C of –6 to –16‰). Using infrared absorption, the TDL system determines the mole fractions of <sup>12</sup>CO<sub>2</sub> and <sup>13</sup>CO<sub>2</sub> independently, rather than their ratio as in mass spectrometry (MS).

The ability of the instrument to measure isotope ratios (δ<sup>13</sup>C) was tested outdoors in a grassland and compared to standard laboratory-based MS measurements made on field-collected flask samples. The TDL was operated at a sampling flow rate of 230 ml min<sup>-1</sup> and a sampling interval of 2 min for two intake heights. There was a consistent offset for δ<sup>13</sup>C of 1.77‰ between the TDL and MS measurements, and the standard deviation of the error (MS – TDL) was 0.35‰ (*n* = 82). Removal of two outliers improved this standard deviation to 0.25‰ (*n* = 80). After removing the offset, 62 out of 82 samples had absolute differences less than 0.3‰. Subsequent laboratory experiments indicated that the TDL/MS offset was caused by pressure broadening, and can be avoided in the future by calibrating the TDL with CO<sub>2</sub> mixed with air rather than nitrogen. Based on these results we estimate the precision for δ<sup>13</sup>C to be 0.25‰ for our sampling scheme. A similar comparison with flask-based measurements of CO<sub>2</sub> mole fraction (<sup>12</sup>CO<sub>2</sub> + <sup>13</sup>CO<sub>2</sub>) made with a calibrated infrared gas analyzer indicated a TDL precision of 0.4% (1.6 μmol mol<sup>-1</sup> at 400 μmol mol<sup>-1</sup>).

The TDL was used to investigate the vertical and temporal variation in the carbon isotope content of respired CO<sub>2</sub> (δ<sup>13</sup>C<sub>R</sub>) from the grassland. Measurements of δ<sup>13</sup>C of CO<sub>2</sub> in air were made during four separate nights at 1 and 60 cm height above ground. δ<sup>13</sup>C<sub>R</sub> did not vary with height, but it did vary from one night to the next. Hourly measurements of δ<sup>13</sup>C<sub>R</sub> showed it changed as much as 6.4‰ (–29.1 ± 0.4 to –22.7 ± 0.8‰) in a single night. Temporal changes in δ<sup>13</sup>C<sub>R</sub> during the night have not been reported in prior studies. Such observations could provide a new way to investigate temporal dynamics of the carbon substrates utilized for ecosystem respiration.

© 2003 Elsevier Science B.V. All rights reserved.

**Keywords:** Carbon cycle; Respiration; TDLAS; Biosphere–atmosphere exchange; Stable isotope

\* Corresponding author. Tel.: +1-801-581-2130; fax: +1-801-581-4665.

E-mail address: [bowling@biology.utah.edu](mailto:bowling@biology.utah.edu) (D.R. Bowling).

## 1. Introduction

The use of stable isotopes in biosphere–atmosphere CO<sub>2</sub> exchange research has increased substantially since Keeling’s pioneering work in the 1950s (Keeling, 1958), especially over the last decade. Stable isotopes of CO<sub>2</sub> have been used at the global scale to investigate the magnitude and nature of carbon exchange between terrestrial ecosystems and the atmosphere (Ciais et al., 1995; Fung et al., 1997; Battle et al., 2000), and at the regional scale to examine large-scale photosynthetic isotope discrimination (Bakwin et al., 1998; Lloyd et al., 2001). Within ecosystems, CO<sub>2</sub> isotopes have been valuable in assessing the proportion of respiratory CO<sub>2</sub> that is “recycled” by photosynthesis (Sternberg, 1989; Sternberg et al., 1997), and investigating the dynamics of the atmospheric surface layer within forest canopies (Bowling et al., 1999). The relative contributions of atmospheric turbulence, photosynthesis, and respiration to isotopic exchange have been addressed (Lloyd et al., 1996; Flanagan et al., 1997), and several studies have attempted to use measurements of isotopic fluxes (<sup>13</sup>CO<sub>2</sub> and C<sup>18</sup>O<sup>16</sup>O) to partition net ecosystem carbon exchange into photosynthetic and respiratory components (Yakir and Wang, 1996; Bowling et al., 2001b, 2003; Ogée et al., 2003).

Many studies have used Keeling plots (Keeling, 1958) to investigate ecosystem physiology. These studies have identified links between the isotope content of CO<sub>2</sub> respired from an ecosystem ( $\delta^{13}\text{C}_R$ ) and environmental drivers, including mean annual precipitation (Pataki et al., 2003), humidity (Ekblad and Höglberg, 2001; Bowling et al., 2002), and soil moisture (Ometto et al., 2002). Collectively, the above studies highlight the importance of stable isotopes of CO<sub>2</sub> as a powerful tool to investigate ecosystem physiology and plant carbon–water relations.

Continuous measurements of CO<sub>2</sub> and ecosystem-scale CO<sub>2</sub> fluxes are now performed at sites all over the world (Valentini et al., 2000; Baldocchi et al., 2001), but so far practical limitations have prevented similar progress for stable isotopes of CO<sub>2</sub>. Every study mentioned above relied on isotope measurements made by laboratory-based isotope ratio mass spectrometry (MS), either in dual-inlet (e.g. Trolier et al., 1996) or continuous flow (Brand, 1996) form. The major limitation to using stable isotopes inten-

sively in biosphere–atmosphere exchange research has been the requirement for samples to be returned to a laboratory for analysis. This has constrained the frequency and duration of isotope sampling in virtually every field application. Development of instrumentation to monitor the isotope content of CO<sub>2</sub> in the field continuously will substantially increase the usefulness of isotopic exchange research to the CO<sub>2</sub> community.

Carbon isotope ratios are expressed relative to an international standard called V-PDB using:

$$\delta^{13}\text{C} = \left( \frac{(^{13}\text{C}/^{12}\text{C})_{\text{sample}}}{(^{13}\text{C}/^{12}\text{C})_{\text{standard}}} - 1 \right) \times 1000. \quad (1)$$

By analogy with percent, the dimensionless “units” used are called permil and denoted ‰. For further details on isotope terminology, see Farquhar et al. (1989). Typical mass spectrometer measurement precisions for  $\delta^{13}\text{C}$  in CO<sub>2</sub> are 0.02–0.1‰ depending on the methods used (Trolier et al., 1996; Ehleringer and Cook, 1998; Ferretti et al., 2000; Ribas-Carbo et al., 2002).

Besides mass spectrometry, a few optical technologies exist for determination of carbon isotope ratios in CO<sub>2</sub>. At present, not all are suitable for atmospheric applications. To be useful in ecosystem–atmosphere stable carbon isotope research, instruments must operate over the CO<sub>2</sub> mole fraction (denoted [CO<sub>2</sub>]) range 350–700  $\mu\text{mol mol}^{-1}$ , and  $\delta^{13}\text{C}$  range –6 to –16‰, with precisions of <1.0  $\mu\text{mol mol}^{-1}$  and <0.5‰. Currently existing technologies include tunable diode laser absorption spectroscopy (TDLAS), with a reported precision for  $\delta^{13}\text{C}$  of 4‰ (Becker et al., 1992), laser optogalvanic effect spectroscopy, with a precision of 0.2‰ for 5% CO<sub>2</sub>-in-N<sub>2</sub> (Murnick and Peer, 1994), Fourier-transform infrared spectroscopy, reporting a precision of 0.1‰ at 350  $\mu\text{mol mol}^{-1}$  CO<sub>2</sub>-in-air (Esler et al., 2000), and TDLAS combined with cavity ring-down spectroscopy with a precision of 0.22‰ for 5% CO<sub>2</sub>-in-N<sub>2</sub> (Crosson et al., 2002). Gas-phase measurements using TDLAS have been reported for carbon and hydrogen isotopes in CH<sub>4</sub> (Bergamaschi et al., 1994) and for oxygen and hydrogen isotopes in water vapor (Kerstel et al., 1999).

A recent review of spectroscopic techniques suitable for micrometeorological applications was provided by Wagner-Riddle et al. (2003). TDLAS is based on absorption of infrared (IR) energy following Beer’s law. A diode laser is tuned to a particular narrow emission

band by controlling the temperature and current applied to the laser. The source wave number is selected to match an individual absorption line on a particular molecule of interest. The laser emission is repeatedly scanned across the entire spectral width of the absorption feature. The line width of the laser emission is typically much smaller than the molecular absorption line width. This allows the instrument to be very selective among components of a gas mixture without interference from other gases, especially at low pressure where the absorption lines are narrower. The source radiation traverses an absorption cell containing sample gas before focusing on a detector. The sensitivity of the analyzer is dependent on the absorption strength of the line chosen and on the absorption path length.

In this paper, we describe in detail a commercially available tunable diode laser system that was adapted to measure  $^{12}\text{CO}_2$  and  $^{13}\text{CO}_2$  in air samples at natural isotopic abundance and mole fractions. We describe the instrument and the conditions under which it was operated, and present results from a field experiment designed to compare the performance of the TDL to the more common mass spectrometer-based approach. We then use the data set obtained during the comparison to evaluate the vertical and temporal dependence of the isotope ratio of whole-ecosystem-respired  $\text{CO}_2$ .

## 2. Methods

### 2.1. TDL system description

The TDL system used in this study was a model TGA100 trace gas analyzer manufactured by Camp-

bell Scientific Inc., Logan, UT. This instrument is based on the original patented design developed by Edwards, Kidd, and Thurtell at the University of Guelph (Edwards et al., 1994). This TDL system design has been used to measure trace gas fluxes of methane, nitrous oxide, and ammonia in several field experiments (Edwards et al., 1994; Wagner-Riddle et al., 1996; Simpson et al., 1997; Billesbach et al., 1998; Warland et al., 2001).

The TGA100 (Fig. 1) includes a tunable lead-salt (SPEC-DILAS single mode DFB, Laser Components, GmbH, Munich, Germany) diode laser (Werle et al., 2002) that is cooled in a liquid nitrogen dewar. The laser is simultaneously temperature and current controlled to produce a linear wavelength scan centered on a single selected absorption line of the target gas. IR radiation produced by the laser is collimated and passed through a 1.5 m single-pass absorption (sample) cell. Pressure in the sample cell is maintained at  $<8$  kPa to keep individual absorption line widths narrow and minimize interference from other gases. A beam splitter directs most of the energy through a focusing lens to the sample detector and reflects a portion of the beam through a second focusing lens and a short reference cell to the reference detector. A prepared reference gas having a known mole fraction of  $\text{CO}_2$  (5%) flows through the reference cell. The reference signal provides a template for the spectral shape of the absorption feature, allowing the mole fraction to be derived without measuring the temperature or pressure of the sample gas or the spectral positions of the scan samples. The reference signal also provides feedback for a digital control algorithm to maintain the center of the spectral scan at the center of the

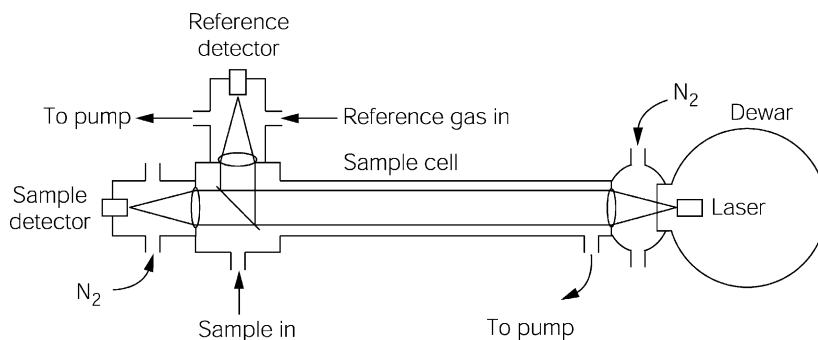


Fig. 1. Diagram of the TGA100 tunable diode laser absorption system.

desired absorption line. The detector signals are amplified and converted in the analyzer electronics, then digitally processed to calculate the mole fraction of the target gas in the sample cell.

The TGA100 was modified to measure both [ $^{12}\text{CO}_2$ ] and [ $^{13}\text{CO}_2$ ] at the same time, and to optimize its performance for the isotope application (in this paper, we use  $[\ ]$  to denote mole fraction by volume in units of  $\mu\text{mol CO}_2 \text{ mol}^{-1}$  of dry air). The TGA100 operating software was modified to measure the two isotopes simultaneously using a jump-scan technique (Fried et al., 1993). In its normal mode, the TGA100 scans a single absorption line 500 times per second, and averages 50 scans to give a mole fraction measurement 10 times per second. The modified software allows the user to specify a laser bias current offset that is applied to every other scan. This offset tunes the source laser output frequency to a different absorption line. For the present study, odd-numbered scans were tuned to a  $^{12}\text{CO}_2$  line and even-numbered scans were tuned to a  $^{13}\text{CO}_2$  line. Even and odd scans were averaged separately, 25 scans each, every 0.1 s. This gave nearly simultaneous mole fraction measurements for each isotope, with an integration time of 98 ms, offset from each other by 2 ms.

The 4 cm space between the laser dewar and the front of the sample cell was sealed and purged with nitrogen gas to avoid absorption by  $\text{CO}_2$  in the ambient air. This purge is not required for trace gases such as  $\text{CH}_4$  and  $\text{N}_2\text{O}$ , because their ambient mole fractions are low and the relevant absorption lines broad at ambient pressure, compared to the much narrower lines at the low pressure maintained in the sample and reference cells. However, even for the very weak  $^{12}\text{CO}_2$  absorption line used in this study, the typical absorption by  $\text{CO}_2$  is an order of magnitude stronger than for  $\text{CH}_4$  or  $\text{N}_2\text{O}$ , requiring purging of the air gap. The sample detector housing was also purged with nitrogen gas.

The TDL measures absorbance, which is proportional to molecular density. The sample mole fraction is inferred by comparing sample absorbance to reference absorbance, assuming the reference and sample gases are at the same temperature (and pressure). The temperature also affects the line strength, i.e. the amount of absorption per molecule. The  $^{12}\text{CO}_2$  and  $^{13}\text{CO}_2$  absorbances increase by 1.5 and 0.1%  $^\circ\text{C}^{-1}$ , respectively, at 40  $^\circ\text{C}$  and 2.1 kPa

(HITRAN high-resolution transmission molecular absorption database, Rothman et al., 1998, [www.hitran.com](http://www.hitran.com)). Because the absorbance depends on temperature, 1  $^\circ\text{C}$  difference in the reference and sample gases can lead to errors of 1.5%, 0.1%, and 14% in [ $^{12}\text{CO}_2$ ], [ $^{13}\text{CO}_2$ ], and  $\delta^{13}\text{C}$ , respectively.

For the above reasons, several modifications were made to maintain the reference and sample gases at the same temperature. The TDL was housed in a fiberglass case with 2.5 cm of insulating foam to dampen diurnal temperature swings and two fans were installed to circulate the air inside the enclosure. The reference and sample gases each flowed through a length of tubing inside the enclosure to bring them to the same temperature before they entered the absorption cells. An insulated cover was placed over the analyzer enclosure and a thermostatically controlled heater was added inside the analyzer enclosure to maintain a more constant temperature. The sample cell was insulated to match the thermal time constant of the reference cell.

The TGA100 operating parameters were optimized for accuracy instead of precision. Typically the TGA100 is used to measure trace gas fluxes using the eddy covariance, flux-gradient, or mass balance techniques. For all of these techniques, a slowly varying offset error has little effect on the measured flux. The measured fluxes are usually small, making the measurement noise a more important factor to overall flux uncertainty than the absolute accuracy. However, measuring isotope ratios with a TDL system requires high mole fraction measurement accuracy for each isotope. The TGA100 optical system was defocused approximately 5 mm to reduce the sensitivity of the optical alignment to temperature changes. This also reduced the signal level, which reduced the effect of detector non-linearity. A relatively low ( $230 \text{ ml min}^{-1}$ ) sample flow rate was chosen to reduce the sample pressure. The low pressure (2.1 kPa) kept the absorption lines narrow, avoiding interference between the closely spaced lines. The low flow rate also minimized calibration gas consumption.

In typical TDLAS applications, absorption lines are chosen based on two criteria: (1) high absorption line strength; and (2) minimal interference from other gases in the sample. This choice determines the particular laser that can be used as an IR source. Additional criteria must be used when selecting absorption lines for isotope ratio measurements. First, there must be a

pair of lines, one for each isotope. Second, lasers have limited tuning ranges, requiring the lines to be close together. Third, the two lines should have similar effective line strengths. The mole fraction of  $^{12}\text{CO}_2$  is approximately 100 times the mole fraction of  $^{13}\text{CO}_2$ ; therefore, the  $^{12}\text{CO}_2$  line should be 100 times weaker than the  $^{13}\text{CO}_2$  line to give a similar absorbance. The TGA100 detector response is slightly non-linear at high signal levels, and the laser emits some of its power at undesired frequencies (multimoding). The TGA100 software corrects for detector non-linearity and laser multimoding, but residual errors affect the measured mole fraction. These errors are dependent on the sample and reference absorbance. Matching the absorbance of the two isotopes increases the correlation of their individual errors, thereby reducing the error in their ratio. Finally, the particular laser used in this study was chosen with the additional constraint that it also operate in the absorption region of the  $^{12}\text{C}^{18}\text{O}^{16}\text{O}$  isotope.

Shown in Fig. 2 are synthetic transmission spectra for  $^{12}\text{CO}_2$  and  $^{13}\text{CO}_2$ , generated using the HITRAN database (Rothman et al., 1998). The general shift in overall broad transmission spectra is apparent for the two isotopes (Fig. 2a). The most suitable pairs of lines are found between 2280 and 2310  $\text{cm}^{-1}$ , where the  $^{13}\text{CO}_2$  lines are strong, and the  $^{12}\text{CO}_2$  lines are weak.

The absorption lines at 2308.570  $\text{cm}^{-1}$  ( $^{12}\text{CO}_2$ ) and 2309.271  $\text{cm}^{-1}$  ( $^{13}\text{CO}_2$ ) were initially chosen (Fig. 2b). This line pair was tested by mixing  $\text{CO}_2$  with nitrogen to give a range of mole fractions with a constant isotope ratio, but was rejected because the measured ratio varied significantly with mole fraction. The  $^{12}\text{CO}_2$  line strength is seven times the  $^{13}\text{CO}_2$  line strength at these wave numbers, reducing the desired correlation of errors caused by detector non-linearity and laser multimoding. Instead, we chose the absorption lines at 2308.225 and 2308.171  $\text{cm}^{-1}$  (wavelengths of 4.332333 and 4.332435  $\mu\text{m}$ ) for  $^{12}\text{CO}_2$  and  $^{13}\text{CO}_2$ , respectively. These lines are close together and better matched in line strength, with the  $^{12}\text{CO}_2$  line strength approximately half the  $^{13}\text{CO}_2$  line strength. They provided virtually no change in measured isotope ratio as a function of mole fraction. These absorption lines each have a small line of the other isotope nearby, with a small influence (<1%) on the measured mole fractions. This error is removed by the calibration process.

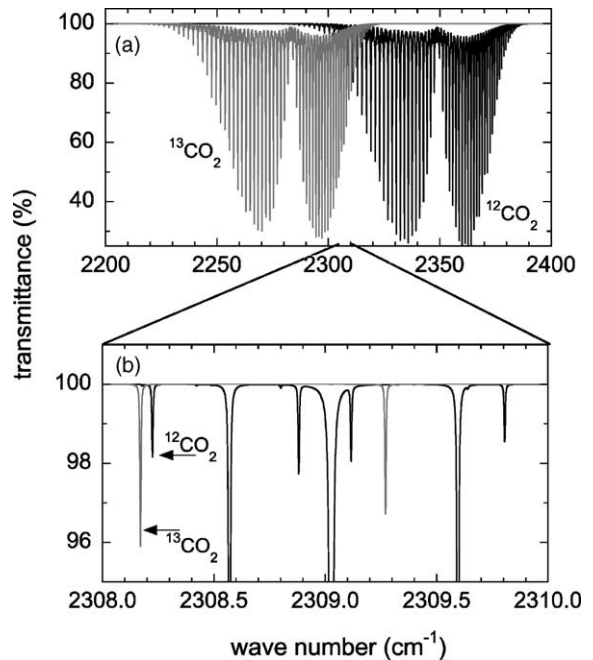


Fig. 2. Transmission spectra for  $^{12}\text{CO}_2$  and  $^{13}\text{CO}_2$ . Shown in (a) are spectra over a broad wave number range; the two right-most lobes are the spectra for  $^{12}\text{CO}_2$ , and the left ones are  $^{13}\text{CO}_2$ . The individual absorption lines used by the TDL for each isotope are shown in (b).

We note that significantly better resolution can be obtained for TDLAS measurements of  $\text{CO}_2$  that are not concerned with isotope ratios. Simpson et al. (1998) used a TGA100 with a short (4.59 cm) sample cell instead of the standard 1.5 m cell to monitor  $[\text{CO}_2]$  at wave numbers between 2350 and 2375  $\text{cm}^{-1}$  (see Fig. 2a), and resolved differences to  $300 \times 10^{-6} \mu\text{mol mol}^{-1}$  over a 30 min averaging time.

## 2.2. Field experiment

### 2.2.1. Site

Field tests of the instrument were conducted in the Cache Valley, near Logan, UT, during 5–10 May 2001. The site (41°45'N, 111°51'W, 1360 m above sea level) was an irrigated agricultural plot on which grass was raised for hay, with no known history of  $\text{C}_4$  crops for more than 20 years. Species growing in 2001 included fescue (*Festuca* spp.), bluegrass (*Poa* spp.), and canary grass (*Phalaris* spp.). Measurements

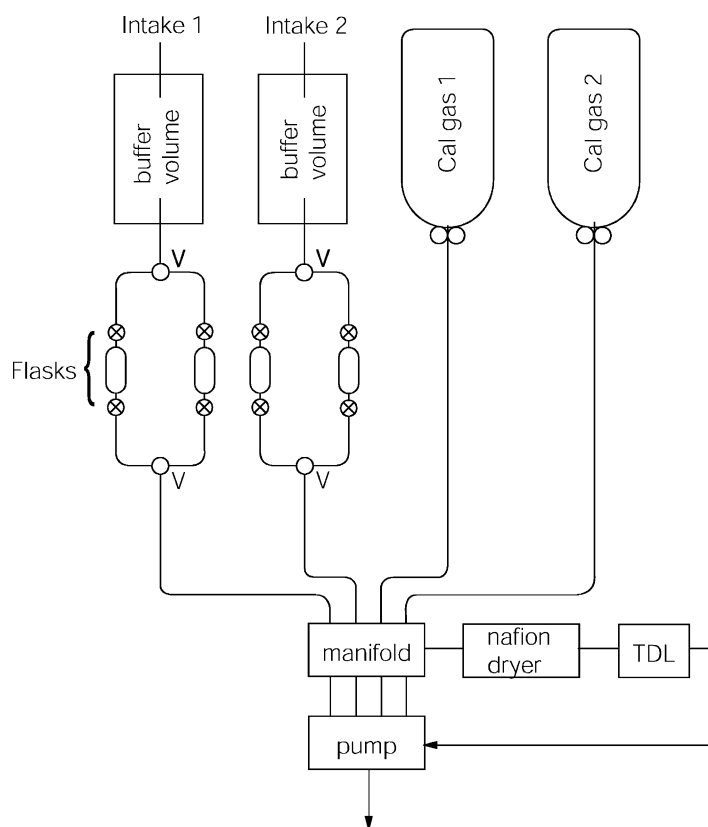


Fig. 3. Diagram of the configuration used in the field to compare TDL measurements with flask collections followed by laboratory mass spectrometer analysis. See Section 2.2.2 for details.

were made at the end of a cold spring and the vegetation canopy was not well developed. Canopy height was measured in 100 locations on a 10-pace grid at  $15.2 \pm 5.4$  cm (mean  $\pm$  S.D.). The field was flat and measured  $800 \text{ m} \times 400 \text{ m}$  (32 ha), and the instruments were located near the center. The weather during the field tests was sunny and clear, with cold nights and warm days. Air temperature during the experiment ranged from  $-1.3$  to  $26.1$  °C. Daytime vapor pressure deficit of air was moderate and peaked at 3.0 kPa.

### 2.2.2. TDL system setup

The TDL system was used outdoors at the site. The TGA100 field measurements were compared to laboratory measurements of mole fraction and isotope ratio made on simultaneously collected flask samples. Tubing (0.64 cm o.d., 12 m long Dekoron, Synflex Specialty Products, Mantua, OH) was used to route

filtered air samples collected at two intake heights (1 and 60 cm above ground) to an assembly of two 10.41 glass buffer volumes (Fig. 3). The volumes were used to dampen rapid changes in  $[\text{CO}_2]$ . Immediately downstream of each buffer volume was a pair of 100 ml glass flasks (34-5671, Kontes Glass Co., Vineland, NJ) in parallel, followed by a critical orifice to control the flow rate (0.018 cm i.d., F-2815-071-B85, Power Aire Inc., Anaheim, CA). A manifold system (Campbell Scientific Inc.) directed one of the four inlets (two sample intakes and two calibration gases) through a Nafion-based drying assembly (PD1000, Campbell Scientific Inc.), and into the TDL system. A pump (RB0021, Busch Inc., Virginia Beach, VA) pulled the air through the entire plumbing system. The flow rate through each inlet was  $230 \text{ ml min}^{-1}$ , with continuous flow in all four air streams, including the calibration gases. The manifold system cycled through the four

air streams every 2 min (intakes 1 and 2, calibration gases 1 and 2), spending 30 s at each intake. The TGA100 data from the last 10 s of each 30 s interval were averaged to measure [ $^{13}\text{CO}_2$ ] and [ $^{12}\text{CO}_2$ ].

The parallel flasks had manual external valves (V, SS-42XS4, Whitey Co., Highland Heights, OH) attached to allow flow through only one flask at a time. When a flask was collected, the valves were used to quickly switch in the alternate flask, and the exact time was recorded. This arrangement allowed us to make a direct comparison between flask samples and TDL measurements with minimal disruption to the sample flow.

The TDL was also used at times without concurrent flask collection, measuring air at two heights (1 and 60 cm), sometimes eliminating the buffer volumes and flasks in Fig. 3. Electrical power was supplied by a gasoline powered generator located roughly 100 m away from the intake lines. The primary focus was on nighttime measurements, so the system was shut down during some days. Problems with the generator caused some data to be lost. In all, TDL system measurements were collected 53% of the time over a period of 4.6 days.

### 2.2.3. Calibration gases and procedure

Three calibration gases were used during the field experiment. Because the TDL measures [ $^{12}\text{CO}_2$ ] and [ $^{13}\text{CO}_2$ ] separately rather than their ratio, values for mole fractions of each isotope were required for each tank. It is not important for the calibration gases to differ in stable isotope ratio, but they should bracket the expected [ $^{12}\text{CO}_2$ ] and [ $^{13}\text{CO}_2$ ] in atmospheric samples.

$\delta^{13}\text{C}$  of all calibration gases was measured at the Stable Isotope Ratio Facility for Environmental Research (SIRFER) at the University of Utah and calibrated to the V-PDB scale using NBS-21 graphite.  $\text{CO}_2$  was purified cryogenically under vacuum from replicate 1.71 flasks;  $\text{N}_2\text{O}$  was removed by catalysis over reduced copper at 500 °C, and  $\delta^{13}\text{C}$  was measured via dual-inlet mass spectrometry (Finnigan MAT 252, Finnigan MAT, San Jose, CA) with a precision of 0.05‰.

$\text{CO}_2$  mole fractions in the three tanks were determined as follows. Tank A was a  $\text{CO}_2$ -in-air mixture (498.4  $\mu\text{mol mol}^{-1}$ , –30.68‰) that was propagated as a secondary  $\text{CO}_2$  calibration standard from a World

Meteorological Organization (WMO) primary tank by infrared gas analysis (IRGA; LI-COR 6262, LI-COR Inc., Lincoln, NE).

Two additional gases, tanks B and C, were used in the field. These were  $\text{CO}_2$ -in- $\text{N}_2$  mixtures (tank B: 363.4  $\mu\text{mol mol}^{-1}$ , –29.55‰; tank C: 1049.0  $\mu\text{mol mol}^{-1}$ , –40.58‰). We could not accurately measure [ $\text{CO}_2$ ] for tanks B and C using the IRGA and WMO primary tank due to the pressure broadening of absorption lines in the presence of  $\text{O}_2$  (Bischof, 1974; Griffith, 1982; Griffith et al., 1982). We used the TGA100 to measure tanks B and C relative to tank A. We measured [ $^{12}\text{CO}_2$ ] from tanks A and B every 2 min over a 30 h period in the field, and used a regression between the measurements to determine [ $^{12}\text{CO}_2$ ] in tank B. We then used carbon isotope ratios measured by dual-inlet mass spectrometry to assign [ $^{13}\text{CO}_2$ ] to tank B. Tank C was calibrated from tank B in a similar fashion.

This method may still introduce an error in [ $^{12}\text{CO}_2$ ] and [ $^{13}\text{CO}_2$ ] for tanks B and C because an air-based calibration tank (A) was used to measure an  $\text{N}_2$ -based tank (B). The TGA100 is likely to be less sensitive to the presence of  $\text{O}_2$  than the IRGA, but pressure broadening is still important. Also, this procedure used a one-point calibration for the TGA100, which did not account for offset errors. Averaging a large number of measurements reduced the effect of the offset error, but a non-zero mean offset may have introduced a bias. Errors in [ $^{12}\text{CO}_2$ ] and [ $^{13}\text{CO}_2$ ] for tanks B and C, and the unknown sensitivity of the TGA100 to the presence of  $\text{O}_2$  in the calibration gas may influence the measured mole fractions and isotope ratios discussed later.

We tested three variations on the above calibration method:

- using regressions based on [ $^{13}\text{CO}_2$ ] instead and assigning [ $^{12}\text{CO}_2$ ] based on isotope ratios measured by dual-inlet mass spectrometry;
- using the mean raw measured values of [ $^{12}\text{CO}_2$ ] in each tank during the 30 h period rather than a regression between them;
- assuming the measured  $\text{CO}_2$  in tank A was made up of  $^{12}\text{CO}_2 + ^{13}\text{CO}_2$ , then arbitrarily assigning  $^{12}\text{CO}_2$  mole fractions equal to half the result—this forces a large (50%) error in mole fraction.

Once the calibration values for each tank were assigned, they were used to adjust raw TDL

measurements as follows. Every 2 min, measurements were made of [ $^{12}\text{CO}_2$ ] and [ $^{13}\text{CO}_2$ ] from two intakes at different sampling heights and two calibration tanks. Gain factors ( $G$ ) and offsets ( $O$ ) were assigned for each isotope:

$$G = \frac{X_C - X_B}{X_{Cm} - X_{Bm}}, \quad (2)$$

$$O = X_C - GX_{Cm}, \quad (3)$$

where  $X_B$  and  $X_C$  are true mole fractions ( $^{12}\text{CO}_2$  or  $^{13}\text{CO}_2$ ) in tanks B and C, and  $X_{Bm}$  and  $X_{Cm}$  the measured mole fractions of each tank. The unknown air samples ( $X_i$ ) were then calculated from the raw ( $X_m$ ) mole fractions using:

$$X_i = X_m G + O. \quad (4)$$

#### 2.2.4. Mass spectrometry and $\text{CO}_2$ mole fraction of flask samples

All flasks were returned to the SIRFER facility for analysis. Carbon isotope ratios of  $\text{CO}_2$  in the flasks were measured using a continuous flow isotope ratio mass spectrometer (IRMS; Finnigan MAT 252, Finnigan MAT, San Jose, CA), as described by Ehleringer and Cook (1998). Precision for  $\delta^{13}\text{C}$  was determined daily by comparison to known standards and was typically  $\pm 0.1\%$ . Corrections for the presence of  $^{17}\text{O}$  were applied, and  $\text{CO}_2$  was separated from  $\text{N}_2\text{O}$  by gas chromatography before analysis. We report all carbon isotope ratio values in this paper relative to the international V-PDB standard. [ $\text{CO}_2$ ] in the flasks was measured using the bellows/IRGA technique of Bowling et al. (2001a,b) with a precision of  $0.3 \mu\text{mol mol}^{-1}$ .

#### 2.2.5. Other equipment

Total  $\text{CO}_2$  mole fraction was measured at 60 and 180 cm height using an IRGA (LI-COR 6262) that was calibrated hourly to a  $399.0 \mu\text{mol mol}^{-1}$   $\text{CO}_2$ -in-air mixture (WMO secondary). Air for this measurement did not flow through buffer volumes. Air was dried before analysis using a Nafion counterflow drying membrane (MD-070-48S, Perma-Pure Inc., Toms River, NJ). All  $\text{CO}_2$  mole fractions in this paper are reported with respect to dry air.

Ambient air temperature and humidity were measured (HMP45C, Vaisala Inc., Woburn, MA) at a height of 1.1 m, inside a naturally aspirated 12-plate radiation shield.

#### 2.2.6. Isotope content of ecosystem respiration ( $\delta^{13}\text{C}_R$ )

The carbon isotope content of ecosystem respiration was determined using the Keeling plot method (Keeling, 1958) and an outlier test and geometric mean regression as outlined in Bowling et al. (2002). Only data with samples covering a [ $\text{CO}_2$ ] range of at least  $75 \mu\text{mol mol}^{-1}$  per Keeling plot were used to minimize the uncertainty in  $\delta^{13}\text{C}_R$  (Pataki et al., 2003).

To evaluate the possible height dependence of  $\delta^{13}\text{C}_R$ , all data collected on four separate nights (6 p.m. to 6 a.m. local time) at a particular sampling height were combined into a single Keeling plot for each night at each height. On the two nights when MS data were available, Keeling plots from these samples were also evaluated, separately from the TDL data.

On three nights, the TDL data were used to investigate the temporal variability of  $\delta^{13}\text{C}_R$ . Data from two sampling heights were combined, and Keeling plots evaluated hourly. There were not enough MS samples to allow a similar hourly analysis of these data.

#### 2.2.7. Pressure broadening experiment

After identifying an offset between MS and TDL measurements during the field experiment (discussed later), a laboratory experiment was performed to study the influence of pressure broadening on TDL performance. Molecular absorption lines are narrow at low pressure and broader at higher pressure. The pressure broadening effect is proportional to pressure and dependent on the gases involved.  $\text{N}_2$ ,  $\text{O}_2$ , and  $\text{H}_2\text{O}$  each cause a different amount of pressure broadening, and the effect differs for each absorption line. Non-dispersive infrared  $\text{CO}_2$  analyzers generally operate near ambient pressure where the pressure broadening effect is largest. However, errors can be minimized by calibrating with  $\text{CO}_2$ -in-air (Bischof, 1974; Griffith, 1982; Griffith et al., 1982), and either drying the sample or applying a correction for pressure broadening by water vapor when samples are not dried. The TDL was operated at low pressure (2.1 kPa) where the pressure broadening effect is relatively small.

In the laboratory, we investigated the effect of using  $\text{CO}_2$ -in- $\text{N}_2$  instead of  $\text{CO}_2$ -in-air calibration gases, which is a pressure-broadening effect due to the presence of  $\text{O}_2$  in air. The TDL was operated similarly to the field experiment, switching between two sample intakes and the calibration gases used in the field

(tanks B and C). The two samples were generated by mixing 5% CO<sub>2</sub>-in-N<sub>2</sub> with either (1) N<sub>2</sub> or (2) ambient air chemically scrubbed of CO<sub>2</sub> and water vapor. The mole fraction of CO<sub>2</sub> was adjusted to approximately 300 or 700 μmol mol<sup>-1</sup> as measured by the TDL using needle valves. The experiment was repeated using the same reference gas used for the field experiment (5% CO<sub>2</sub>-in-N<sub>2</sub>) and a tank of 5% CO<sub>2</sub>-in-air. No attempt was made to independently determine the actual mole fraction of CO<sub>2</sub> in the samples, as purpose of this experiment was to measure the effect on the isotope ratio only. The mole fractions in the samples were calculated as discussed in Section 3.2.

### 3. Results and discussion

#### 3.1. Laboratory tests

##### 3.1.1. Stability over time

Preliminary experiments showed that the TGA100 requires frequent calibration to achieve the accuracy required for isotope ratio measurements. In the laboratory, the instrument was used to measure mole fractions of each isotope from a compressed air cylinder every 100 ms for 13.9 h (Fig. 4a). The standard deviation as a percentage of the mean of measured [<sup>12</sup>CO<sub>2</sub>] and [<sup>13</sup>CO<sub>2</sub>] over this time were 0.33 and 0.12%, respectively, at relatively constant instrument temperatures. Although this level of noise is acceptable in most atmospheric trace gas measurement applications, it is not acceptable for isotope ratio applications unless the errors in [<sup>12</sup>CO<sub>2</sub>] and [<sup>13</sup>CO<sub>2</sub>] are highly correlated. If the errors in the mole fractions are completely uncorrelated, the uncertainty in their ratio ( $\delta R$ ) will be  $\delta R/|R| = ((0.0033)^2 + (0.0012)^2)^{0.5}$  (Taylor, 1982) where  $|R|$  is the absolute value of the mean ratio  $R$ . This gives 0.35% or 3.5‰, in good agreement with the actual standard deviation of the time series of the isotope ratio, 3.6‰ (data not shown), indicating the errors in measured [<sup>12</sup>CO<sub>2</sub>] and [<sup>13</sup>CO<sub>2</sub>] were not correlated. Hence, the accurate measurement of small isotope differences in atmospheric CO<sub>2</sub> requires additional considerations, particularly in the field.

We used the Allan variance, or two-sample variance (Allan, 1966) to examine temporal changes in instrument response and to define a calibration strat-

egy. The application of the Allan variance to TDLAS has been discussed in detail (Werle et al., 1993), so we only briefly mention it here. Imagine a situation where a constant process with random instrument error is measured over some time period, e.g. [<sup>12</sup>CO<sub>2</sub>] in a compressed gas cylinder. If the statistics of the measurement error are constant in time (stationary), then averaging the instrument response for longer time periods will provide a smaller variance (higher measurement precision). A log–log plot of the ordinary variance versus averaging time for this hypothetical measurement of [<sup>12</sup>CO<sub>2</sub>] would show a constant decrease in proportion to the averaging time (dashed lines in Fig. 4b).

However, if other factors such as temperature drift cause the statistics of the error to change, averaging over longer periods will eventually cause the variance to increase. The Allan variance is useful when the long-term (low frequency) statistics of a random process are not constant, i.e. non-stationary. The Allan variances of the time series in Fig. 4a are shown in Fig. 4b. For averaging times <30 s, increasing the averaging time decreases the variance as predicted, following the theoretical slope. However, the variance begins to increase for averaging times >30 s as other factors influence the instrument noise. This provides a measure of the optimal averaging time (Werle et al., 1993). This analysis (Fig. 4b) shows that to minimize the error in measured mole fractions of each isotope, averaging times of tens of seconds need to be used and calibrations performed approximately every minute. The practical considerations of monitoring two intakes and two calibration gases led us to select the 2 min calibration scheme described in Section 2.

##### 3.1.2. Potential for making measurements of $\delta^{18}O$

Although the focus of our experiment was on carbon isotopes, this TDL configuration can potentially be used to measure the stable oxygen isotope content ( $\delta^{18}O$ ) of CO<sub>2</sub>, which is also useful in ecosystem carbon cycle studies (e.g. Flanagan et al., 1997). The intercept of the Allan variance plot (Fig. 4b) gives a practical method to measure the short-term noise excluding the effect of the long-term drift. The short-term noise for carbon isotope ratios in our laboratory experiment was 1.5‰ (data not shown). Laboratory experiments using the absorption lines at 2308.416 cm<sup>-1</sup> for <sup>12</sup>C<sup>18</sup>O<sup>16</sup>O and 2308.570 cm<sup>-1</sup>

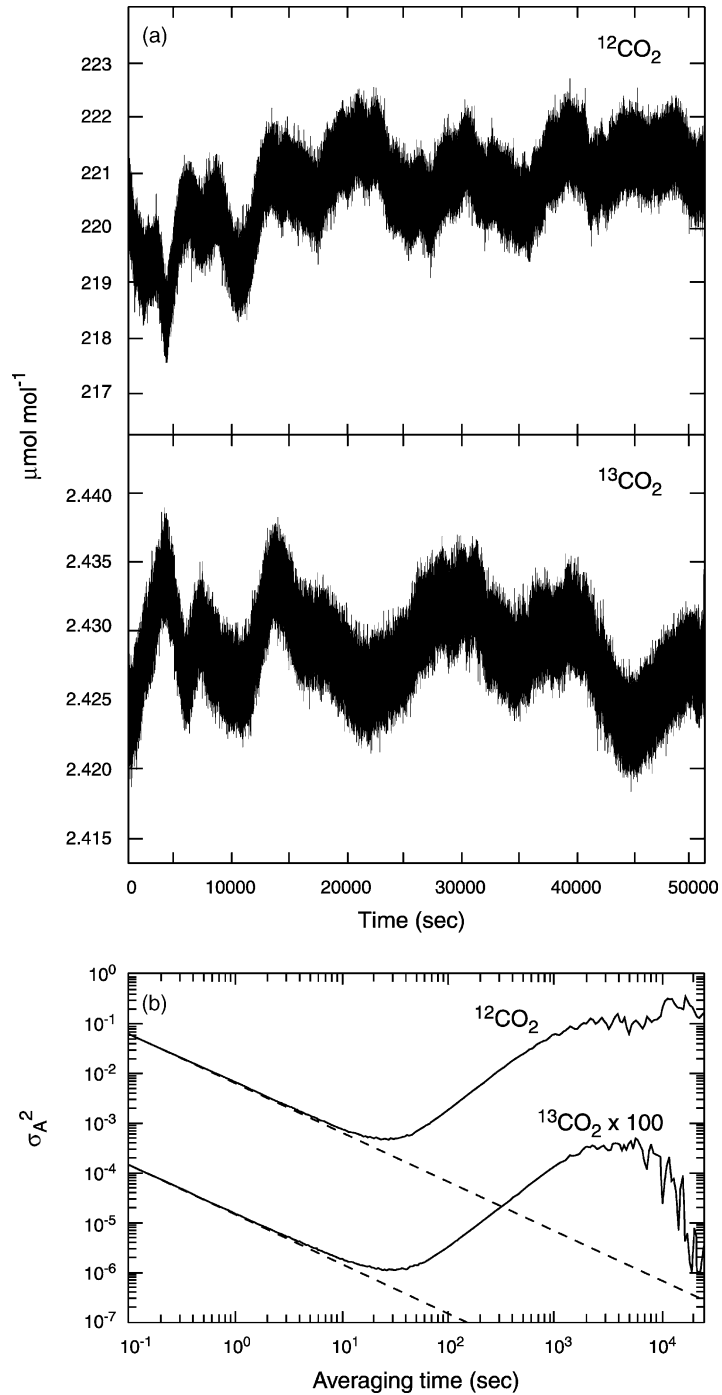


Fig. 4. (a) Time series of  $^{12}\text{CO}_2$  and  $^{13}\text{CO}_2$  measured every 100 ms from a compressed air cylinder with the TDL in the laboratory. The data were not calibrated. (b) Allan variances of the time series in (a). The dashed lines represent the theoretical slope associated with a stationary random process. The Allan variance for  $^{13}\text{CO}_2$  has been multiplied by 100.

for  $^{12}\text{C}^{16}\text{O}_2$  gave a short-term noise for the ratio ( $^{12}\text{C}^{18}\text{O}^{16}\text{O}/^{12}\text{C}^{16}\text{O}_2$ ) of 2.2‰ (expressed as  $\delta^{18}\text{O}$ ). In general, we found the noise when measuring  $\delta^{18}\text{O}$  was roughly 50% greater than the noise for  $\delta^{13}\text{C}$ . We did not make comparisons to mass spectrometer measurements, but this noise performance suggests the TDL may also be useful for measuring oxygen isotope ratios. The use of a different tunable laser or different absorption lines might lead to better sensitivity for  $^{12}\text{C}^{18}\text{O}^{16}\text{O}$ .

### 3.2. Field experiment

#### 3.2.1. Gain and offset calibration factors

The TDL system was used outdoors for the field experiment and experienced large ( $>25^\circ\text{C}$ ) diurnal changes in air temperature. Considerable variation was observed in measured (raw) mole fractions of the calibration gases. The gain factors calculated using Eq. (2) for each isotope varied on a diurnal basis by up to 3% (Fig. 5), with a larger range for  $^{12}\text{CO}_2$  than  $^{13}\text{CO}_2$ . These gain factors were strongly correlated with air temperature and showed evidence of hysteresis, with

a stronger relationship during increasing temperature (morning) than when the air was cooling in the evening (data not shown). Variation was also observed in the calibration offsets given by Eq. (3) (Fig. 5).

The TDL gain variation (Fig. 5a) was likely caused by a combination of effects related to temperature. In spite of the thermostatically controlled heater inside the analyzer enclosure, the temperature of the sample and reference cells typically varied by 3 and  $5^\circ\text{C}$  throughout the day. This difference in temperature between the sample and reference cells would cause a corresponding difference in the absorption line strengths, leading to errors in  $[\text{CO}_2]$  and  $[\text{CO}_2]$ . The errors in  $[\text{CO}_2]$  were larger than the errors in  $[\text{CO}_2]$  because the  $^{12}\text{CO}_2$  absorption line strength varies more with temperature than the  $^{13}\text{CO}_2$  line.

Other instrument effects may also have contributed to the change in gain. Detector non-linearity is a function of the total optical flux density on the detector, which depends on temperature in several ways. First, blackbody emissions from the walls of the optical path vary strongly with temperature, and contribute to the total optical power on the detectors. Second,

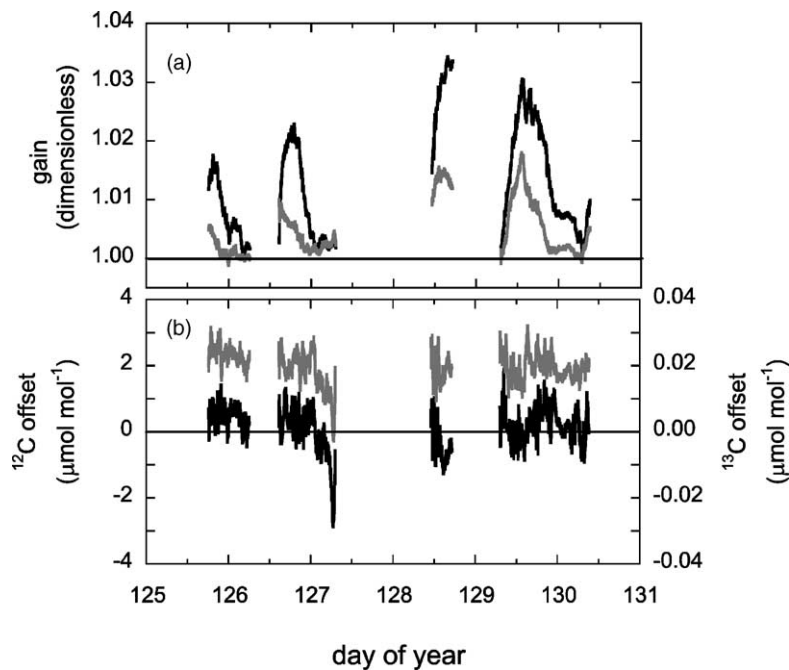


Fig. 5. Calibration gain factors (a) and offsets (b) for  $^{12}\text{CO}_2$  (black line) and  $^{13}\text{CO}_2$  (gray line) during the field experiment. Gains and offsets were calculated using Eqs. (2) and (3).

the flux density from the laser is affected by optical alignment, which may change slightly with temperature. The laser is physically mounted to a very finely temperature-controlled (within 0.001 K) plate inside the laser dewar. However, the temperature of the laser itself is influenced by blackbody emissions from the optical window, dewar walls, and the inside of the analyzer enclosure viewed by the laser through the optical window. As the temperature of the laser changes, its bias current is automatically adjusted to maintain the correct emission frequency. The laser bias current varied approximately 1.5 mA throughout the day. The laser's optical power output depends on the bias current, leading to measurement errors due to detector non-linearity.

The actual change in laser temperature corresponding to the 1.5 mA change in bias current is estimated to be 0.13 K, based on the laser's current and temperature tuning rates ( $0.06 \text{ cm}^{-1} \text{ mA}^{-1}$  and  $0.7 \text{ cm}^{-1} \text{ K}^{-1}$ ). This change in temperature may have affected the errors due to multimoding, which tends to vary with laser temperature. Based on laboratory experiments, the laser used in this experiment emitted approximately 98% of its power at the desired frequency, and the other 2% at some unknown frequency (data not shown). This multimode laser emission gives an error in the reported mole fraction that is dependent on the amount of multimode power and the absorbance of the sample and reference gases. The TGA100 performs a correction for this multimode laser emission, but the residual error in this correction would change if the laser's multimode emission changed with temperature.

The TDL offset variation was likely associated with Fabry–Perot interference fringing caused by undesired reflections along the laser's optical path. The reflected IR signal can interfere either constructively or destructively with the unreflected signal, depending on the path length of the reflection and the wavelength of the laser's output. This modulates the laser signal as a function of wavelength, leading to a mole fraction offset error that changes slowly over time, as the reflection path length changes with temperature. Early TGA100 analyzers showed large offsets (e.g. Billesbach et al., 1998). More recent TGA100 analyzers reduce the amplitude of the offset errors through better data reduction algorithms and hardware modifications, but this offset

error remains significant for absolute mole fraction measurements.

These results, combined with the Allan variance analysis (Fig. 4b) highlight the importance of frequent (every 2 min) measurement of calibration gases for isotope applications of the TDL. If the gain and offset variations are adequately characterized they are easily calibrated away.

### 3.2.2. Time series

Calibrated time series of [ $^{12}\text{CO}_2$ ], [ $^{13}\text{CO}_2$ ], their sum, and their ratio (expressed as  $\delta^{13}\text{C}$  using Eq. (1)) measured by the TDL on a typical night are shown in Fig. 6. These data were collected at two above-canopy heights, and clearly show the nocturnal buildup of respiratory  $\text{CO}_2$  from the grassland. Note that there was approximately 1.1% as much  $^{13}\text{CO}_2$  (range 4–7  $\mu\text{mol mol}^{-1}$ ) as there was  $^{12}\text{CO}_2$ . The relative proportion of the lighter  $\text{CO}_2$  carbon isotope is always roughly 1.1%. As the heavy isotope increases in mole fraction, the lighter isotope also increases in mole fraction, but there are very small changes in the relative proportions of each (their isotope ratio, Fig. 6d). This is a subtle but important point. Isotope ratio variation (in  $\delta$  notation) of  $-8$  to  $-16\text{‰}$  (a large range for the atmosphere) corresponds to values of the absolute isotope ratio ( $^{13}\text{CO}_2/^{12}\text{CO}_2$ ) of only 0.01106–0.01115 (Eq. (1)).

The dynamics of the increase of mole fractions of each isotope were similar in pattern, but not identical. When the individual mole fractions were summed, the comparison with IRGA measurements was quite favorable (Fig. 6c). The isotope ratios at each height generally decreased over the night, consistent with the well-established addition of respiratory  $\text{CO}_2$  of lighter isotope content (less  $^{13}\text{C}$  relative to  $^{12}\text{C}$ , corresponding to more negative  $\delta^{13}\text{C}$ ) to the atmosphere (e.g. Flanagan et al., 1996). The intake closer to the ground showed more negative  $\delta^{13}\text{C}$  as expected. There was considerable temporal variation in  $\delta^{13}\text{C}$  of atmospheric  $\text{CO}_2$  during the course of a single night. Capturing this variation with flask collections and mass spectrometry would be impractical. There are 938 individual measurements of  $\delta^{13}\text{C}$  shown in Fig. 6d, collected at two heights every 2 min. Analysis of this many flask samples would require a mass spectrometer in our laboratory operating 24 h a day for 13 days, and a massive experimental effort in the field.

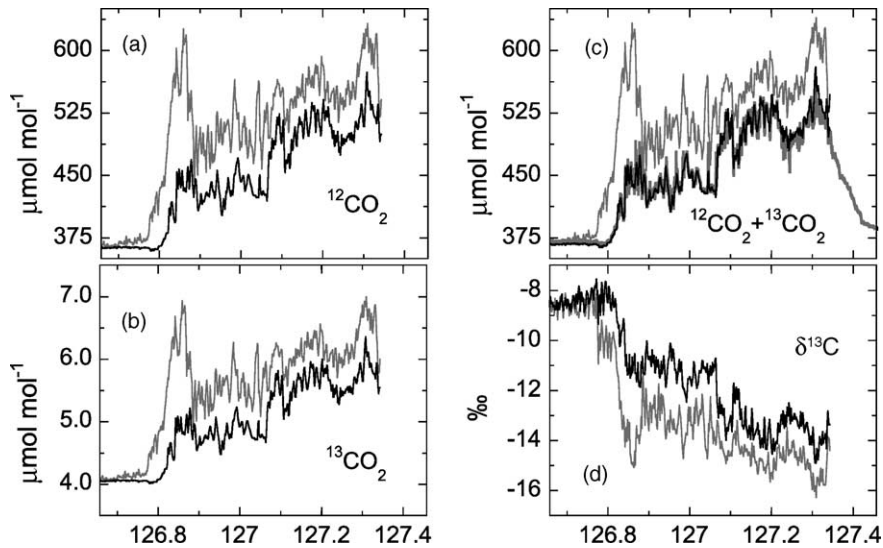


Fig. 6. Time series of TDL measurements of (a) [ $^{12}\text{CO}_2$ ], (b) [ $^{13}\text{CO}_2$ ], (c) [ $^{12}\text{CO}_2$ ] + [ $^{13}\text{CO}_2$ ], and (d)  $\delta^{13}\text{C}$  measured at two heights (1 cm, gray lines; 60 cm, black lines) during the night of 6 and 7 May. The data in panels (a) and (b) were used (via Eq. (1)) to calculate initial  $\delta^{13}\text{C}$  values, then a constant offset of 1.77‰ was subtracted from the  $\delta^{13}\text{C}$  values to produce the data in (d). Also shown in (c) is a time series of [ $\text{CO}_2$ ] measured with an IRGA at 60 cm (thick gray line).

### 3.2.3. Comparison with flask samples

A  $\text{CO}_2$  mole fraction comparison between TDL measurements in the field and concurrent flask collections followed by measurement of the flasks with an IRGA in the laboratory is shown in Fig. 7a.  $\text{CO}_2$  is measured in WMO primary standards manometrically (Zhao et al., 1997) so all  $\text{CO}_2$  isotopes ( $^{12}\text{C}^{16}\text{O}_2$ ,  $^{13}\text{C}^{16}\text{O}_2$ ,  $^{12}\text{C}^{18}\text{O}^{16}\text{O}$ ,  $^{12}\text{C}^{17}\text{O}^{16}\text{O}$ , etc.) contribute fully to the WMO  $\text{CO}_2$  value. Because the IRGA-based measurements were WMO traceable, they also reflect the contribution of all isotopic variants. The TDL measurements are limited to  $^{12}\text{C}^{16}\text{O}_2$  and  $^{13}\text{C}^{16}\text{O}_2$  only, which make up most but not all (99.526%) carbon dioxide (Hoefs, 1997). Thus, the minor isotopes  $^{12}\text{C}^{18}\text{O}^{16}\text{O}$ ,  $^{12}\text{C}^{17}\text{O}^{16}\text{O}$ , etc. contribute 0.474%, or 1.9 out of 400  $\mu\text{mol mol}^{-1}$ . The TDL data in Fig. 7a were adjusted by this factor (the y-axis equals ( $[^{12}\text{CO}_2] + [^{13}\text{CO}_2]$ )  $\times 100/99.526$ ) to compare the TDL measurements to the IRGA measurements.

In total there were 81 samples available for comparison between the two methods (82 for  $\delta^{13}\text{C}$  due to an error in [ $\text{CO}_2$ ] measurement of one flask), and all available data are shown in Fig. 7. The average mole fraction error (flask – TDL) was 2.3  $\mu\text{mol mol}^{-1}$ ,

and the standard deviation (S.D.) of this error was 5.6  $\mu\text{mol mol}^{-1}$  ( $n = 81$ ). On average, the error in a  $\text{CO}_2$  mole fraction measurement made by the TDL was 0.6%. Excluding the two points with the most extreme error changed the mean and S.D. to 1.6 and 2.8  $\mu\text{mol mol}^{-1}$ , respectively, and the percent error to 0.4% ( $n = 79$ ). The flask data were not used at any step in the calibration of the TDL.

The comparison between isotope ratios measured in the field with the TDL and concurrent flask collections followed by MS analysis is shown in Fig. 7b. Samples were collected for comparison over a large [ $\text{CO}_2$ ] range of 357.3–699.7  $\mu\text{mol mol}^{-1}$ , and a proportionally large  $\delta^{13}\text{C}$  range of  $-7.5$  to  $-16.3$ ‰. The standard deviation of the  $\delta^{13}\text{C}$  difference between the methods (MS – TDL) was 0.35‰ ( $n = 82$ ). Removal of the two outliers at the top-left (Fig. 7b) decreased the standard deviation to 0.25‰ ( $n = 80$ ; the outliers were the same data points as in Fig. 7a). Based on these results, we estimate the precision of the TDL isotope ratio measurements to be 0.25‰. This precision is worse than the mass spectrometer precision of 0.02–0.1‰, but considering the 2 min sampling frequency of the TDL and logistical problems associated with flask sampling, the TDL precision is clearly acceptable.

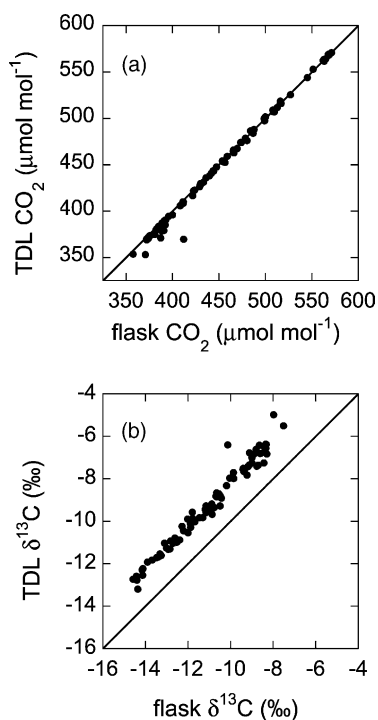


Fig. 7. (a) Comparison of  $[\text{CO}_2]$  in air measured using field-collected flask samples followed by IRGA measurement of the flasks in the laboratory, and the TDL in the field. The TDL data are the sum of  $^{12}\text{CO}_2$  and  $^{13}\text{CO}_2$ , adjusted for other minor isotopes as described in the text. (b) Comparison of carbon isotope ratios between the flask samples combined with MS and the TDL. The 1:1 line is shown for comparison.

There was an isotopic offset of  $1.77\text{‰}$  between samples analyzed by the two methods, which was constant over the wide range of  $\delta^{13}\text{C}$  values observed. Samples were collected over a large range of air temperatures that strongly influenced the raw measured mole frac-

tions. However, the frequent measurement of two calibration gases permitted temperature-based effects to be removed using the gain factors and offsets in Fig. 5, resulting in a constant TDL/MS offset.

Was the offset caused by pressure broadening due to the presence of  $\text{O}_2$  in our samples and the lack of  $\text{O}_2$  in our calibration gases? The results of the pressure broadening experiment are summarized in Table 1. The difference in isotope ratios is consistent in magnitude with the offset observed in the field experiment. When  $\text{CO}_2$ -in- $\text{N}_2$  calibration gases were used in the field, measured isotope ratios of unknown air samples were more positive than MS measurements by  $1.77\text{‰}$  (Fig. 7). In Table 1, when the same  $\text{CO}_2$ -in- $\text{N}_2$  calibration gases were used in the laboratory, measured isotope ratios of  $\text{CO}_2$ -in-air samples were more positive than  $\text{CO}_2$ -in- $\text{N}_2$  samples by roughly the same amount ( $1.51$ – $1.78\text{‰}$ ). There was no significant difference in this result when the reference gas was  $\text{CO}_2$ -in- $\text{N}_2$  or  $\text{CO}_2$ -in-air. Additional experiments were performed with and without the presence of water vapor in the measured gases (data not shown), and pressure broadening due to water vapor was also observed.

The  $\delta^{13}\text{C}$  offset is not a consequence of inter-laboratory calibration differences—all isotope ratio measurements of calibration gases were made in the same laboratory. It seems clear from the pressure broadening experiment (Table 1) that the offset is a direct result of our use of  $\text{CO}_2$ -in- $\text{N}_2$  calibration gases in the field.

Our  $^{12}\text{CO}_2$  measurement of tank B was based on a field comparison between tanks A (containing  $\text{O}_2$ ) and B (with no  $\text{O}_2$ ). This tank was used to calibrate  $^{12}\text{CO}_2$  in tank C, and tanks B and C were used as calibration standards to generate the TDL data shown in Fig. 7. As discussed, this means that  $^{12}\text{CO}_2$  in tanks

Table 1

Difference in  $\delta^{13}\text{C}$  measured by TDL for mixtures of either  $\text{CO}_2$ -free air or  $\text{N}_2$  and 5%  $\text{CO}_2$ -in- $\text{N}_2$ , diluted to atmospheric mole fractions

| Reference gas | $\text{CO}_2$ -in-air                           |                           |                                   | $\text{CO}_2$ -in- $\text{N}_2$                 |                           |                                   | $n$ | $\delta^{13}\text{C}$ difference (air – $\text{N}_2$ ) (‰) |
|---------------|---|---------------------------|-----------------------------------|---|---------------------------|-----------------------------------|-----|--|
|               | $^{12}\text{CO}_2$ ( $\mu\text{mol mol}^{-1}$ ) | $\delta^{13}\text{C}$ (‰) | S.D. of $\delta^{13}\text{C}$ (‰) | $^{12}\text{CO}_2$ ( $\mu\text{mol mol}^{-1}$ ) | $\delta^{13}\text{C}$ (‰) | S.D. of $\delta^{13}\text{C}$ (‰) |     |  |
| $\text{N}_2$  | 345   | –33.18                    | 0.46                              | 328   | –34.69                    | 0.39                              | 11  | 1.51   |
| $\text{N}_2$  | 672   | –33.17                    | 0.50                              | 661   | –34.95                    | 0.46                              | 12  | 1.78   |
| Air           | 298   | –33.09                    | 0.31                              | 291   | –34.86                    | 0.31                              | 12  | 1.77   |
| Air           | 714   | –33.43                    | 0.46                              | 707   | –35.06                    | 0.41                              | 12  | 1.63   |

Also shown are  $^{12}\text{CO}_2$ ,  $\delta^{13}\text{C}$ , the standard deviation of  $\delta^{13}\text{C}$  for each mixture, and the number of samples ( $n$ ).

B and C were not well known. When variations on our calibration scheme were examined (see Section 2), very little difference in the overall TDL/MS isotope ratio offset in Fig. 7 was observed (data not shown). The range of offsets obtained from all calibration variations was 1.76–1.85‰. In the most extreme case, the [ $^{12}\text{CO}_2$ ] and [ $^{13}\text{CO}_2$ ] values assigned for tanks B and C were forced to be in error by 50%, but the isotope ratio offset was only 1.76‰. Because the measured isotope ratios of the calibration tanks were preserved in each scheme, the final  $\delta^{13}\text{C}$  results were quite similar regardless of the mole fraction values assigned to the calibration tanks.

Of course, error in determination of [ $^{12}\text{CO}_2$ ] and [ $^{13}\text{CO}_2$ ] in the calibration tanks will cause a proportional error in measured mole fraction of unknown samples. However, the isotope ratio comparison with MS measurements was excellent after correction for the offset (Figs. 7 and 8). Following standard practice in the scientific community for IRGA measurements (Bischof, 1974; Griffith, 1982; Griffith et al.,

1982; Zhao et al., 1997), we recommend using only  $\text{CO}_2$ -in-air calibration gases for TDL measurements of carbon isotopes. We recommend drying the sample to avoid differences in the pressure broadening effect due to sample humidity. We also recommend that a frequent calibration scheme such as the one outlined here be employed.

Time series TDL data with the offset subtracted are shown in Fig. 8. MS samples during this period are also shown. The temporal patterns in mole fraction and in isotope ratio that were observed with the MS samples are clearly seen in the TDL measurements, and a favorable comparison is apparent at both measurement heights. IRGA measurements at 60 cm are shown for comparison. The TDL and flask measurements were made on air that had been buffered by mixing volumes (Fig. 3), dampening the rapid fluctuations seen in the unbuffered IRGA measurements. The results shown in Figs. 7 and 8 provide strong evidence that the TDL measurements are accurate and can reliably reproduce temporal and spatial trends in atmospheric  $\delta^{13}\text{C}$ .

#### 3.2.4. Spatial and temporal variation in $\delta^{13}\text{C}_R$

We used the data in a Keeling plot analysis to investigate variation in the carbon isotope ratio of ecosystem-respired  $\text{CO}_2$ . Those unfamiliar with Keeling plots are directed to a recent review of their application in ecosystem carbon research (Pataki et al., 2003). Several studies have observed substantial variation in  $\delta^{13}\text{C}_R$  over a season (Buchmann et al., 1997; Bowling et al., 2002; Fessenden and Ehleringer, 2002; Ometto et al., 2002; Mortazavi and Chanton, 2002), but the extent to which  $\delta^{13}\text{C}_R$  might vary spatially within an ecosystem or over the course of several hours has not been established, primarily because of the difficulty in collecting enough flask samples over a short time period.

Because the stable nocturnal boundary layer inhibits vertical mixing, it is reasonable to assume that air samples collected near the ground, within, and above a vegetation canopy will be influenced by different biota. Foliar respiration is likely to be a product of oxidation of recently fixed carbon, whereas the below-ground and litter respiration components may have a substantial contribution from heterotrophic decomposition of carbon substrates of varying age. Hence the isotope content of respiration may vary with height. Keeling plots at different heights from the present

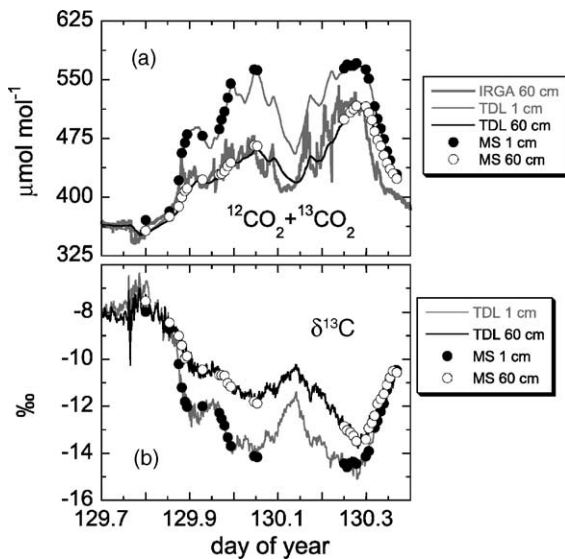


Fig. 8. Comparison of time series of [ $\text{CO}_2$ ] and  $\delta^{13}\text{C}$  measured using the TDL (lines) and MS (symbols) at two heights (1 and 60 cm) during the night of 9 and 10 May. An offset of 1.77‰ has been subtracted from the TDL  $\delta^{13}\text{C}$  data. Also shown in (a) is [ $\text{CO}_2$ ] measured at 60 cm using an IRGA (thick gray line). The high frequency fluctuations in the IRGA measurements were damped in the TDL and MS measurements due to the use of buffer volumes (Fig. 3).

Table 2

Height dependence of Keeling plot intercepts ( $\delta^{13}\text{C}_R$ ) and slopes and their standard error (S.E.)

| Night      | Sampling height (cm) | $\delta^{13}\text{C}_R$ (‰) | S.E. of $\delta^{13}\text{C}_R$ (‰) | Slope (‰ $\mu\text{mol mol}^{-1}$ ) | S.E. of slope (‰ $\mu\text{mol mol}^{-1}$ ) | $n$ | $r^2$ | $\text{CO}_2$ range ( $\mu\text{mol mol}^{-1}$ ) |
|------------|----------------------|-----------------------------|-------------------------------------|-------------------------------------|---|-----|-------|--|
| 125        | 1                    | -27.18                      | 0.08                                | 6906.3                              | 32.7  | 290 | 0.994 | 176.2  |
| 125        | 60                   | -27.57                      | 0.12                                | 7080.5                              | 47.0  | 290 | 0.987 | 120.3  |
| Difference |                      | 0.39                        | 0.20                                |                                     |   |     |       |  |
| 126        | 1                    | -27.38                      | 0.07                                | 7135.4                              | 34.7  | 245 | 0.994 | 228.7  |
| 126        | 60                   | -27.20                      | 0.08                                | 7032.2                              | 36.3  | 297 | 0.992 | 183.7  |
| Difference |                      | -0.18                       | 0.15                                |                                     |   |     |       |  |
| 128 (MS)   | 1                    | -25.41                      | 0.48                                | 6422.1                              | 256.9                                       | 12  | 0.984 | 324.3  |
| 128 (MS)   | 60                   | -25.37                      | 0.22                                | 6334.4                              | 100.5                                       | 11  | 0.998 | 241.8  |
| Difference |                      | -0.04                       | 0.70                                |                                     |   |     |       |  |
| 129        | 1                    | -25.55                      | 0.07                                | 6360.5                              | 36.2  | 266 | 0.991 | 208.0  |
| 129        | 60                   | -25.88                      | 0.10                                | 6488.0                              | 43.5  | 266 | 0.988 | 142.4  |
| Difference |                      | 0.33                        | 0.17                                |                                     |   |     |       |  |
| 129 (MS)   | 1                    | -25.91                      | 0.11                                | 6643.9                              | 51.5  | 12  | 0.999 | 192.2  |
| 129 (MS)   | 60                   | -26.10                      | 0.20                                | 6642.4                              | 83.1  | 13  | 0.998 | 108.6  |
| Difference |                      | 0.19                        | 0.31                                |                                     |   |     |       |  |

Data are from geometric mean regressions of an entire night (6 p.m. to 6 a.m.) with sampling heights evaluated separately. Also shown are the number of samples in the regression ( $n$ ), the coefficient of determination ( $r^2$ ), and the  $\text{CO}_2$  range of the samples. Data are from TDL measurements in the field except where flasks were collected and analyzed by mass spectrometry. The night column represents the evening that measurements began (125 is the night of days 125 and 126). The two values below each pair are the difference in  $\delta^{13}\text{C}_R$  at the two heights and sum of the standard errors of each (which is the uncertainty of their difference).

study are shown in Table 2. Within a single night, the largest height difference observed in  $\delta^{13}\text{C}_R$  was  $0.39 \pm 0.20\%$ . The uncertainty in the individual intercepts is inversely related to the range of  $\text{CO}_2$  in samples collected (Pataki et al., 2003); these ranges are among the highest reported, leading to very small uncertainties in  $\delta^{13}\text{C}_R$  (0.07–0.48‰). Given our instrument precision (0.25‰), we cannot distinguish any of the differences in Table 2 from zero. However, Ogée et al. (2003) reported considerable variation in  $\delta^{13}\text{C}_R$  with height in a pine (*Pinus pinaster*) forest in France, so our observations probably do not indicate a general pattern.

There were, however, differences in  $\delta^{13}\text{C}_R$  between nights, a range of 2.2‰, from -25.37 to -27.57‰ (Table 2). Bowling et al. (2002) observed that ecosystem respiration was enriched in  $^{13}\text{C}$  (more positive  $\delta^{13}\text{C}_R$ ) in coniferous forests when air was sampled following freezing air temperatures and suggested that the cause was related to stomatal closure in response to cold temperatures followed by a decrease in photo-

synthetic carbon isotope discrimination. In the present study, the air temperature dropped below zero during the early morning hours of day 128 (night 127), and  $\delta^{13}\text{C}_R$  on nights 128 and 129 was relatively more positive than it had been previously, lending some support to their hypothesis.

When TDL data from all heights were combined and analyzed on an hourly basis, substantial variation in  $\delta^{13}\text{C}_R$  was observed (Fig. 9). Within a single night (126), Keeling plot intercepts varied from -22.68 to -29.08‰. The magnitude of this variation (6.4‰) is nearly as large as the seasonal ranges reported over a wide variety of environmental conditions from several years of sampling in Oregon coniferous forests (3.5–8.5‰; Bowling et al., 2002). There was a common trend on two of the three nights, with more positive  $\delta^{13}\text{C}_R$  early in the evening, decreasing gradually over the night. Such a trend might be expected if: (1) autotrophic respiration made up a substantial proportion of total ecosystem respiration; (2) photosynthetic discrimination decreased over the course of the

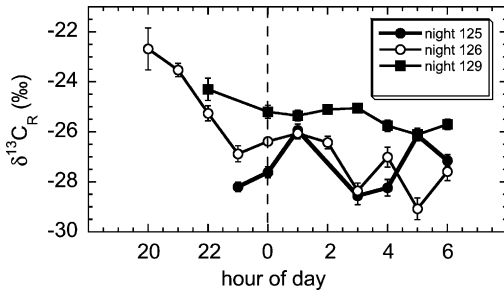


Fig. 9. Temporal changes in  $\delta^{13}\text{C}_R$  over the course of three nights (the nights begin in the evening of days 125, 126 and 129). Each point represents the intercept of a Keeling plot made on samples collected over 1 h with data from two heights (1 and 60 cm) combined. Only intercepts from Keeling plots with  $\text{CO}_2$  ranges greater than  $75 \mu\text{mol mol}^{-1}$  are shown. A vertical dashed line is shown at midnight. Error bars are smaller than the symbols in some cases.

day, leading to enrichment in  $^{13}\text{C}$  of photosynthetic compounds created during daylight hours and subsequently respired at night; and/or (3) the substrate for autotrophic respiration early in the evening was recent photosynthate (fixed during the last several hours) and slowly changed to stored carbon substrates as the night progressed.

These limited data suggest that there can be large temporal variation in  $\delta^{13}\text{C}_R$  within a single night, a finding that has not been previously reported. At present, the use of isotopic fluxes to partition net ecosystem carbon exchange is dependent on the existence of a temporal isotopic disequilibrium between photosynthetic carbon assimilation and respiratory release (i.e. the isotope content of the gross photosynthetic and respiratory fluxes are different; Bowling et al., 2001b, 2003). This does not necessarily mean that the fluxes will differ isotopically over a longer integration time (e.g. 24 h), but they must differ isotopically on a time scale of hours for isotopic partitioning of net ecosystem exchange to work on the same time scale.

Bowling et al. (2003) estimated the isotopic composition of the photosynthetic flux and showed that it is not constant over the daylight period. Our results suggest that the carbon isotopic composition of the nocturnal respiratory flux may not be constant either. If this is true, then there could be substantial information about both components of ecosystem carbon exchange contained in this variation.

## 4. Conclusions

We have measured the carbon isotope content of  $\text{CO}_2$  in air at atmospheric mole fractions and isotopic abundances using a commercially available tunable diode laser absorption spectrometer. By comparison with standard laboratory-based mass spectrometry, we have demonstrated that with regular calibration the TDL can operate with a precision of 0.25‰ for two intakes with a 2 min sampling interval. The TDL is suitable for use in the field and can provide continuous, unattended measurements. This sampling frequency is unprecedented in ecosystem-atmosphere stable isotope research.

## Acknowledgements

Thanks to Laurence Rothman and colleagues at the Harvard-Smithsonian Center for Astrophysics for maintaining the HITRAN database. Russ Monson provided considerable scientific and logistical insight in the early stages of this research. We are grateful to Ray Cartee and the Utah Agricultural Experiment Station at Utah State University for access to the site. Andy Schauer, Ed Swiatek, and Bruce Smith provided assistance with field work. Craig Cook, Mike Lott, Andy Schauer, and Cane Grande generously provided their time and analytical expertise. This material is based upon work supported by the National Science Foundation under Grant No. 9905717. Any opinions, findings, and conclusions or recommendations expressed in this material are those of the author(s) and do not necessarily reflect the views of the National Science Foundation.

## References

- Allan, D.W., 1966. Statistics of atomic frequency standards. *Proc. IEEE* 54, 221–231.
- Bakwin, P.S., Tans, P.P., White, J.W.C., Andres, R.J., 1998. Determination of the isotopic ( $^{13}\text{C}/^{12}\text{C}$ ) discrimination by terrestrial biology from a global network of observations. *Global Biogeochem. Cycles* 12, 555–562.
- Baldocchi, D.D., et al., 2001. FLUXNET: a new tool to study the temporal and spatial variability of ecosystem-scale carbon dioxide, water vapor, and energy flux densities. *Bull. Am. Meteorol. Soc.* 11, 2415–2434.

- Battle, M., Bender, M.L., Tans, P.P., White, J.W.C., Ellis, J.T., Conway, T., Francey, R.J., 2000. Global carbon sinks and their variability inferred from atmospheric O<sub>2</sub> and δ<sup>13</sup>C. *Science* 287, 2467–2470.
- Becker, J.F., Sauke, T.B., Loewenstein, M., 1992. Stable isotope analysis using tunable diode laser spectroscopy. *Appl. Opt.* 31, 1921–1927.
- Bergamaschi, P., Schupp, M., Harris, G.W., 1994. High-precision direct measurements of <sup>13</sup>CH<sub>4</sub>/<sup>12</sup>CH<sub>4</sub> and <sup>12</sup>CH<sub>3</sub>D/<sup>12</sup>CH<sub>4</sub> ratios in atmospheric methane sources by means of a long-path tunable diode laser absorption spectrometer. *Appl. Opt.* 33, 7704–7716.
- Billesbach, D.P., Kim, J., Clement, R.J., Verma, S.B., Ullman, F.G., 1998. An intercomparison of two tunable diode laser spectrometers used for eddy correlation measurements of methane flux in a prairie wetland. *J. Atmos. Ocean. Technol.* 15, 197–198.
- Bischof, W., 1974. The influence of the carrier gas on the infrared gas analysis of atmospheric CO<sub>2</sub>. *Tellus* 27, 59–61.
- Bowling, D.R., Baldocchi, D.D., Monson, R.K., 1999. Dynamics of isotopic exchange of carbon dioxide in a Tennessee deciduous forest. *Global Biogeochem. Cycles* 13, 903–922.
- Bowling, D.R., Cook, C.S., Ehleringer, J.R., 2001a. Technique to measure CO<sub>2</sub> mixing ratio in small flasks with a bellows/IRGA system. *Agric. For. Meteorol.* 109, 61–65.
- Bowling, D.R., Tans, P.P., Monson, R.K., 2001b. Partitioning net ecosystem carbon exchange with isotopic fluxes of CO<sub>2</sub>. *Global Change Biol.* 7, 127–145.
- Bowling, D.R., McDowell, N.G., Bond, B.J., Law, B.E., Ehleringer, J.R., 2002. <sup>13</sup>C content of ecosystem respiration is linked to precipitation and vapor pressure deficit. *Oecologia* 131, 113–124.
- Bowling, D.R., Pataki, D.E., Ehleringer, J.R., 2003. Critical evaluation of micrometeorological methods for measuring ecosystem–atmosphere isotopic exchange of CO<sub>2</sub>. *Agric. For. Meteorol.* 116, 159–179.
- Brand, W.A., 1996. High precision isotope ratio monitoring techniques in mass spectrometry. *J. Mass Spectrom.* 31, 225–235.
- Buchmann, N., Kao, W.-Y., Ehleringer, J., 1997. Influence of stand structure on carbon-13 of vegetation, soils, and canopy air within deciduous and evergreen forests in Utah, United States. *Oecologia* 110, 109–119.
- Ciais, P., Tans, P.P., Trolier, M., White, J.W.C., Francey, R.J., 1995. A large northern hemisphere terrestrial CO<sub>2</sub> sink indicated by the <sup>13</sup>C/<sup>12</sup>C ratio of atmospheric CO<sub>2</sub>. *Science* 269, 1098–1102.
- Crosson, E.R., et al., 2002. Stable isotope ratios using cavity ring-down spectroscopy: determination of <sup>13</sup>C/<sup>12</sup>C for carbon dioxide in human breath. *Anal. Chem.* 74, 2003–2007.
- Edwards, G.C., Neumann, H.H., den Hartog, G., Thurtell, G.W., Kidd, G., 1994. Eddy correlation measurements of methane fluxes using a tunable diode laser at the Kinosheo Lake tower site during the Northern Wetlands Study (NOWES). *J. Geophys. Res.* 99, 1511–1517.
- Ehleringer, J.R., Cook, C.S., 1998. Carbon and oxygen isotope ratios of ecosystem respiration along an Oregon conifer transect: preliminary observations based on small-flask sampling. *Tree Physiol.* 18, 513–519.
- Eklblad, A., Högberg, P., 2001. Natural abundance of <sup>13</sup>C in CO<sub>2</sub> respired from forest soils reveals speed of link between tree photosynthesis and root respiration. *Oecologia* 127, 305–308.
- Esler, M.B., Griffith, D.W.T., Wilson, S.R., Steele, L.P., 2000. Precision trace gas analysis by FT-IR spectroscopy. 2. The <sup>13</sup>C/<sup>12</sup>C isotope ratio of CO<sub>2</sub>. *Anal. Chem.* 72, 216–221.
- Farquhar, G.D., Ehleringer, J.R., Hubick, K.T., 1989. Carbon isotope discrimination and photosynthesis. *Annu. Rev. Physiol. Plant Mol. Biol.* 40, 503–537.
- Ferretti, D.F., Lowe, D.C., Martin, R.J., Brailsford, G.W., 2000. A new gas chromatograph–isotope ratio mass spectrometry technique for high-precision, N<sub>2</sub>O-free analysis of δ<sup>13</sup>C and δ<sup>18</sup>O in atmospheric CO<sub>2</sub> from small air samples. *J. Geophys. Res.* 105, 6709–6718.
- Fessenden, J.E., Ehleringer, J.R., 2002. Age-related variations in δ<sup>13</sup>C of ecosystem respiration across a coniferous forest chronosequence in the Pacific Northwest. *Tree Physiol.* 22, 159–167.
- Flanagan, L.B., Brooks, J.R., Varney, G.T., Berry, S.C., Ehleringer, J.R., 1996. Carbon isotope discrimination during photosynthesis and the isotope ratio of respired CO<sub>2</sub> in boreal forest ecosystems. *Global Biogeochem. Cycles* 10, 629–640.
- Flanagan, L.B., Brooks, J.R., Varney, G.T., Ehleringer, J.R., 1997. Discrimination against C<sup>18</sup>O<sup>16</sup>O during photosynthesis and the oxygen isotope ratio of respired CO<sub>2</sub> in boreal forest ecosystems. *Global Biogeochem. Cycles* 11, 83–98.
- Fried, A., Henry, B., Drummond, J.R., 1993. Tunable diode laser ratio measurements of atmospheric constituents by employing dual fitting analysis and jump scanning. *Appl. Opt.* 32, 821–827.
- Fung, I., Field, C.B., Berry, J.A., Thompson, M.V., Randerson, J.T., Malmström, C.M., Vitousek, P.M., Collatz, G.J., Sellers, P.J., Randall, D.A., Denning, A.S., Badeck, F., John, J., 1997. Carbon-13 exchanges between the atmosphere and the biosphere. *Global Biogeochem. Cycles* 11, 507–533.
- Griffith, D.W.T., 1982. Calculations of carrier gas effects in non-dispersive infrared analyzers. I. Theory. *Tellus* 34, 376–384.
- Griffith, D.W.T., Keeling, C.D., Adams, J.A., Guenther, P.R., Bacastow, R.B., 1982. Calculations of carrier gas effects in non-dispersive infrared analyzers. II. Comparisons with experiment. *Tellus* 34, 385–397.
- Hoefs, J., 1997. *Stable Isotope Geochemistry*. Springer, Berlin, 201 pp.
- Keeling, C.D., 1958. The concentrations and isotopic abundances of atmospheric carbon dioxide in rural areas. *Geochim. Cosmochim. Acta* 13, 322–334.
- Kerstel, E.R.T., van Trigt, R., Dam, N., Reuss, J., Meijer, H.A.J., 1999. Simultaneous determination of the <sup>2</sup>H/<sup>1</sup>H, <sup>17</sup>O/<sup>16</sup>O, and <sup>18</sup>O/<sup>16</sup>O isotope abundance ratios in water by means of laser spectrometry. *Anal. Chem.* 71, 5297–5303.
- Lloyd, J., Kruijt, B., Hollinger, D.Y., Grace, J., Francey, R., Wong, S.-C., Kelliher, F.M., Miranda, A.C., Farquhar, G.D., Gash, J.H.C., Vygodskaya, N.N., Wright, I.R., Miranda, H.S., Schulze, E.-D., 1996. Vegetation effects on the isotopic composition

- of atmospheric CO<sub>2</sub> at local and regional scales: theoretical aspects and a comparison between rain forest in Amazonia and a boreal forest in Siberia. *Aust. J. Plant. Physiol.* 23, 371–399.
- Lloyd, J., Francey, R.J., Mollicone, D., Raupach, M.R., Sogachev, A., Arneeth, A., Byers, J.N., Kelliher, F.M., Rebmann, C., Valentini, R., Wong, S.-C., Bauer, G., Schulze, E.-D., 2001. Vertical profiles, boundary layer budgets, and regional flux estimates for CO<sub>2</sub> and its <sup>13</sup>C/<sup>12</sup>C ratio and for water vapor above a forest/bog mosaic in central Siberia. *Global Biogeochem. Cycles* 15, 267–284.
- Mortazavi, B., Chanton, J.P., 2002. Carbon isotopic discrimination and control of nighttime canopy δ<sup>18</sup>O–CO<sub>2</sub> in a pine forest in the southeastern United States. *Global Biogeochem. Cycles* 16, doi: 10.1029/2000GB001390.
- Murnick, D.E., Peer, B.J., 1994. Laser-based analysis of carbon isotope ratios. *Science* 263, 945–947.
- Ogé, J., Peylin, P., Ciais, P., Bariac, T., Brunet, Y., Berbigier, P., Roche, C., Richard, P., Bardoux, G., Bonnefond, J.-M., 2003. Partitioning net ecosystem carbon exchange into net assimilation and respiration using <sup>13</sup>CO<sub>2</sub> measurements: a cost-effective sampling strategy. *Global Biogeochem. Cycles* (in press).
- Ometto, J.P.H.B., Flanagan, L.B., Martinelli, L.A., Moreira, M.Z., Higuchi, N., Ehleringer, J.R., 2002. Carbon isotope discrimination in forest and pasture ecosystems of the Amazon Basin Brazil. *Global Biogeochem. Cycles* 16, 1109, doi: 10.1029/2001GB001462.
- Pataki, D.E., Ehleringer, J.R., Flanagan, L.B., Yakir, D., Bowling, D.R., Still, C.J., Buchmann, N., Kaplan, J.O., Berry, J.A., 2003. The application and interpretation of Keeling plots in terrestrial carbon cycle research. *Global Biogeochem. Cycles* 17, 1022, doi: 10.1029/2001GB001850.
- Ribas-Carbo, M., Still, C., Berry, J., 2002. Automated system for simultaneous analysis of δ<sup>13</sup>C, δ<sup>18</sup>O and CO<sub>2</sub> concentrations in small air samples. *Rapid Commun. Mass Spectrom.* 16, 339–345.
- Rothman, I.S., et al., 1998. The HITRAN molecular spectroscopic database and HAWKS (HITRAN Atmospheric Workstation): 1996 edition. *J. Quant. Spectrosc. Radiat. Transfer* 60, 665–710.
- Simpson, I.J., Edwards, G.C., Thurtell, G.W., den Hartog, G., Neumann, H.H., Staebler, R.M., 1997. Micrometeorological measurements of methane and nitrous oxide exchange above a boreal aspen forest. *J. Geophys. Res.* 102, 29331–29341.
- Simpson, I.J., Thurtell, G.W., Neumann, H.H., den Hartog, G., Edwards, G.C., 1998. The validity of similarity theory in the roughness sublayer above forests. *Boundary Layer Meteorol.* 87, 69–99.
- Sternberg, L.S.L., 1989. A model to estimate carbon dioxide recycling in forests using <sup>13</sup>C/<sup>12</sup>C ratios and concentrations of ambient carbon dioxide. *Agric. For. Meteorol.* 48, 163–173.
- Sternberg, L.S.L., Moreira, M.Z., Martinelli, L.A., Victoria, R.L., Barbosa, E.M., Bonates, L.C.M., Nepstad, D.C., 1997. Carbon dioxide recycling in two Amazonian tropical forests. *Agric. For. Meteorol.* 88, 259–268.
- Taylor, J.R., 1982. *An Introduction to Error Analysis*. University Science Books, Mill Valley, 270 pp.
- Trolier, M., White, J.W.C., Tans, P.P., Masarie, K.A., Gemery, P.A., 1996. Monitoring the isotopic composition of atmospheric CO<sub>2</sub>: measurements from the NOAA Global Air Sampling Network. *J. Geophys. Res.* 101, 25897–25916.
- Valentini, R., et al., 2000. Respiration as the main determinant of carbon balance in European forests. *Nature* 404, 861–865.
- Wagner-Riddle, C., Thurtell, G.W., Kidd, G.E., Edwards, G.C., Simpson, I.J., 1996. Micrometeorological measurements of trace gas fluxes from agricultural and natural ecosystems. *Infrared Phys. Technol.* 37, 51–58.
- Wagner-Riddle, C., Edwards, G.C., Thurtell, G.W., 2003. Trace gas concentration measurements for micrometeorological flux quantification. In: Hatfield, J. (Ed.) *Micrometeorological Measurements in Agricultural Systems*. Agronomy Monograph, ASA, CSSA, and SSSA, Madison, WI (in press).
- Warland, J.S., Dias, G.M., Thurtell, G.W., 2001. A tunable laser diode system for ammonia flux measurements over multiple plots. *Environ. Pollut.* 114, 215–221.
- Werle, P., Mücke, R., Slemr, F., 1993. The limits of signal averaging in atmospheric trace-gas monitoring by tunable diode-laser absorption spectroscopy. *Appl. Phys. B* 57, 131–139.
- Werle, P., Slemr, F., Maurer, K., Kormann, R., Mücke, R., Jänker, B., 2002. Near- and mid-infrared laser-optical sensors for gas analysis. *Opt. Lasers Eng.* 37, 101–114.
- Yakir, D., Wang, X.F., 1996. Fluxes of CO<sub>2</sub> and water between terrestrial vegetation and the atmosphere estimated from isotope measurements. *Nature* 380, 515–517.
- Zhao, C.L., Tans, P.P., Thoning, K.W., 1997. A high precision manometric system for absolute calibrations of CO<sub>2</sub> in dry air. *J. Geophys. Res.* 102, 5885–5894.